Adaptive Robust Data-driven Building Control via Bi-level Reformulation: an Experimental Result

Yingzhao Lian†, Jicheng Shi†, Manuel Koch and Colin N.Jones*

***Abstract*— Data-driven control approaches for the minimization of energy consumption of buildings have the potential to significantly reduce deployment costs and increase uptake of advanced control in this sector. A number of recent approaches based on the application of Willems' fundamental lemma for data-driven controller design from input/output measurements are very promising for deterministic LTI systems. This paper addresses the key noise-free assumption, and extends these data-driven control schemes to adaptive building control with measured process noise and unknown measurement noise via a robust bilevel formulation, whose upper level ensures robustness and whose lower level guarantees prediction quality. Corresponding numerical improvements and an active excitation mechanism are proposed to enable a computationally efficient reliable operation. The efficacy of the proposed scheme is validated by a numerical example and a real-world experiment on a single-zone conference building on the EPFL campus. The real-world experiment includes a 20-day non-stop test, where, without extra modeling effort, our proposed controller improves 18% energy efficiency against an industry-standard controller, while also robustly ensures occupant comfort.**

***Index Terms*— Robust Data-driven Control, Experimental Building Control**

I. Introduction

Predictive control techniques have recently been proven to be effective for controlling building HVAC systems with reduced energy consumption while simultaneously improving comfort. However, the cost of model building and commissioning has proven to be very high and as a result, data-driven approaches for building energy saving have been receiving broad attention.

The motivation of this work is to develop a practical robust adaptive data-driven building controller, whose time-varying linear dynamics are disturbed by measurable process noise including outdoor temperature and solar radiation, and whose output measurements are contaminated by unknown measurement noise. Beyond building control, systems with measurable disturbances are ubiquitous, especially in energy-related applications: solar radiation in photovoltaic power systems, electricity demand in power grids, and power generation in airborne wind energy systems, to name a few. The main contributions of this paper are summarized as follows:

- Propose a tractable adaptive robust bi-level data-driven building controller, which decouples data-driven trajectory prediction from control input decisions.
- Propose an active excitation mechanism to ensure data quality while maintaining robust building operation.
- Experimental validation of the proposed scheme on a real-world building.

Previous Work

Data can be used to model building dynamics [12] or to directly generate/improve control policies. Due to seasonal variations [4] and component wear, building dynamics are usually slowly time-varying, and adaptive model predictive control (MPC) has been introduced to combine online parameter estimation and control in [22]. For example, the experiment in [46] adaptively estimated the model of an evaporator in the HVAC system, which was then used to control the valve set-points. [34] ran an extended Kalman filter to achieve online parameter adaptation before the estimated model was used in an MPC controller. However, these parameter-estimation-based adaptive methods usually require a-priori knowledge about the structure of the building dynamics and/or the HVAC systems.

Beyond running through a modeling/estimation procedure, data can be used to refine a control policy. The main approaches in this direction include reinforcement learning (RL) [44] and iterative learning control (ILC) [14]. In particular, ILC has been used for buildings with fixed heating/occupant schedules [38], [52] and RL for learning a building control policy that is not necessarily iterative. To run these learning schemes, a high-fidelity building simulator is usually required, and therefore publications on successful experiments with HVAC systems are rare, with two exceptions being [15], [39].

Beyond RL and ILC, data can also be used to directly characterize a system's response from a behavioral theoretic viewpoint [49]. Willems' fundamental lemma is such a tool that provides a characterization of linear time invariant (LTI)

This work was supported by the Swiss National Science Foundation under the RISK project (Risk Aware Data-Driven Demand Response), grant number 200021 175627

†: First two authors contribute equally. In particular, Yingzhao Lian is responsible for the framework of this work and Jicheng Shi is responsible for the experiment.

*: Corresponding author

Yingzhao Lian, Jicheng Shi, Manuel Koch and Colin Neil Jones are with the Automatic Control Lab, EPFL, Switzerland.(e-mail: {yingzhao.lian, jicheng.shi, manuelpascal.koch, colin.jones}@epfl.ch)

systems from measured input and output trajectories. Such a characterization offers a convenient interface to data-driven controller design [16], [18], [36], [37]. Motivated by the simplicity and effectiveness of the fundamental lemma, its extension to a more general setting is attracting broad attention, including nonlinear extensions [7], [11], [32], [42] and the relaxation of the persistent excitation condition [55].

However, even for LTI systems, the absence of output measurement noise in the standard Willems' fundamental lemma limits its practicality and, hence, a wide range of researchers are studying this challenge [8], [9], [17], [47], [51]. To the best of the authors' knowledge, most previous work in this area make a number of unrealistic assumptions. For example, the signal to noise ratio in the numerical result of [9] is 10^6, which is effectively noise free. The regularizers in [17] and [20, p. 19] reach 10^5, thus overpowering the penalty on the tracking error (Details in Section II). [8], [18], [47], [48] consider a model with process noise and measurement-noise-free fully measurable states, but this assumption partially negates the necessity of data-driven methods. While [51] considers a system with measurement noise, the Hankel matrices are assumed to be noise-free. It is noteworthy to point out that no real-world experimental result is available except for [10], [23]. However, [23] uses an MPC regulator to generate the data used for the data-driven regulator, which limits its application, as a model is still required. Instead of solving the general case, this paper focuses on the applications with unknown measurement noise and measurable process noise, and building control is one of these applications (see Section. II-B for more details).

In the following, Wassertein distance, Willems' fundamental lemma and its corresponding predictive control problem are reviewed in Section II, accompanied by a more in-depth motivation of this paper. A novel robust version of this data-driven controller based on bi-level optimization is introduced in Section III, whose adaptive extension is introduced in Section IV. The mathematical implications of the corresponding lower level problem is summarized in Lemma 2 and the numerical details about the adaptive update and computational improvement are discussed in Section IV-B. Finally, an active excitation mechanism is introduced in Section IV-A, where Algorithm 1 summarizes the complete adaptive robust data-driven controller proposed in this paper. The effectiveness of the proposed algorithm is first validated through simulation with a simple example in Section V, followed by the experimental results with an entire building on the EFPL campus in Section VI. A conclusion of this paper is given in Section VII.

Notation: $\mathcal{N}(\mu, \Sigma)$ denotes a Gaussian distribution with mean μ and covariance Σ. $\otimes$ is the symbol for the Kronecker product. $\times$ is the symbol for the set product operation, $\oplus$ is the symbol of Minkowski sum and $\ominus$ is the symbol of Pontryakin difference. colspan(A) denotes the column space (*e.g.* range) of the matrix A. I_n is the $n \times n$ identity matrix and $\mathbf{O}$ is a matrix of all zeros. $\|\cdot\|$ denotes the Euclidean two-norm. $x := \{x_i\}_{i=1}^T$ denotes a sequence of size T indexed by i. x_i denotes the measurement of x at time i, and $x_{1:L} := [x_1^\top, x_2^\top \dots x_L^\top]^\top$ denotes a concatenated sequence of x_i ranging from x_1 to x_L, and we drop the index to improve clarity if the intention is clear from the context.

II. Preliminaries

Definition 1: A Hankel matrix of depth L associated with a vector-valued signal sequence $s := \{s_i\}_{i=1}^T$, $s_i \in \mathbb{R}^{n_s}$ is

$$\mathfrak{H}_L(s) := \begin{bmatrix} s_1 & s_2 & \dots & s_{T-L+1} \\ s_2 & s_3 & \dots & s_{T-L+2} \\ \vdots & \vdots & & \vdots \\ s_L & s_{L+1} & \dots & s_T \end{bmatrix} .$$

A deterministic linear time-invariant (LTI) system, dubbed $\mathfrak{B}(A, B, C, D)$, is defined as

$$x_{i+1} = Ax_i + Bu_i \ , \ y_i = Cx_i + Du_i \ , \tag{1}$$

whose order is denoted by $\mathfrak{D}(\mathfrak{B}(A, B, C, D)) := n_x$ and n_u, n_y denotes its input and output dimensions respectively. An L-step trajectory generated by this system is

$$[u_{1:L}, y_{1:L}] := [u_1^\top, \dots, u_L^\top, y_1^\top, \dots, y_L^\top]^\top .$$

The set of all possible L-step trajectories generated by $\mathfrak{B}(A, B, C, D)$ is denoted by $\mathfrak{B}_L(A, B, C, D)$.

Given a sequence of input-output measurements $\{u_{\mathbf{d},i}, y_{\mathbf{d},i}\}_{i=1}^T$, we call the input sequence persistently exciting of order L if $\mathfrak{H}_L(u_\mathbf{d})$ is full row rank. By building the following n_c-column stacked Hankel matrix

$$\mathfrak{H}_L(u_\mathbf{d}, y_\mathbf{d}) := \begin{bmatrix} \mathfrak{H}_L(u_\mathbf{d}) \\ \mathfrak{H}_L(y_\mathbf{d}) \end{bmatrix} , \tag{2}$$

we state **Willems' Fundamental Lemma** as

Lemma 1: [50, Theorem 1] Consider a controllable linear system and assume $\{u_\mathbf{d}\}_{i=1}^T$ is persistently exciting of order $L + \mathfrak{O}(\mathfrak{B}(A, B, C, D))$. The condition colspan$(\mathfrak{H}_L(u_\mathbf{d}, y_\mathbf{d})) = \mathfrak{B}_L(A, B, C, D)$ holds.

For the sake of consistency, a datapoint coming from the training dataset is marked by boldface subscript $_\mathbf{d}$. L is reserved for the length of the system responses and n_c denotes the number of columns in a Hankel matrix.

A data-driven control scheme has been proposed in [16], [36], where Lemma 1 generates a trajectory prediction within the following predictive control problem,

$$\min_{y_{pred}, u_{pred}, g} \ J(y_{pred}, u_{pred}) + \underbrace{\eta_g \|g\| + \eta_\sigma \|\sigma\|}_{(a)} \tag{3a}$$

$$\text{s.t.} \ \begin{bmatrix} \mathfrak{H}_{L,init}(y_\mathbf{d}) \\ \mathfrak{H}_{L,init}(u_\mathbf{d}) \\ \mathfrak{H}_{L,pred}(u_\mathbf{d}) \\ \mathfrak{H}_{L,pred}(y_\mathbf{d}) \end{bmatrix} g = \begin{bmatrix} y_{init} + \sigma \\ u_{init} \\ u_{pred} \\ y_{pred} \end{bmatrix} \tag{3b}$$

$$u_{pred} \in \mathcal{U} \ , \ y_{pred} \in \mathcal{Y} \ ,$$

where $J(\cdot, \cdot)$ is a strongly convex objective function, $\mathcal{U}$ and $\mathcal{Y}$ denote compact convex constraint sets on the input and the output. u_{init}, y_{init} are a t_{init}-step sequence of measured inputs

and outputs preceding the current point in time. The matrix $\mathfrak{H}_L(y_{\mathbf{d}})$ is split into two sub-Hankel matrices as

$$\mathfrak{H}_L(y_{\mathbf{d}}) = \begin{bmatrix} \mathfrak{H}_{L,init}(y_{\mathbf{d}}) \\ \mathfrak{H}_{L,pred}(y_{\mathbf{d}}) \end{bmatrix} .$$

The matrix $\mathfrak{H}_{L,init}(y_{\mathbf{d}})$ is of depth t_{init} and the depth of $\mathfrak{H}_{L,pred}(y_{\mathbf{d}})$ is the prediction horizon n_h such that $t_{init}+n_h = L$. Hence, y_{pred} is the predictive output sequence viewed from the current point in time. The matrices $\mathfrak{H}_{L,init}(u_{\mathbf{d}})$, $\mathfrak{H}_{L,pred}(u_{\mathbf{d}})$ are defined accordingly. The choice of t_{init} is made to ensure a unique estimation of the initial state; please refer to [37] for more details.

The last two terms (a) in the objective (3a) are reported as an engineering heuristic to alleviate the impact of measurement noise and model mismatch [16], where η_g and η_σ are user-defined parameters. However, based on our experiments and the parameters reported in [16], [20], [23], [30], if the output measurement data $y_{\mathbf{d}}$ is noisy or the model is not perfectly LTI, η_g and η_σ often must be tuned to unreasonably large values in order to maintain an acceptable control performance. Notice that [54] proposed a maximum likelihood based method to adapt η_g and η_σ via a non-convex optimization problem, but the proposed heuristic algorithm lacks a convergence guarantee. From an intuitive viewpoint, a key issue with the predictive scheme (3) is that it couples the trajectory prediction problem and the optimal control problem into a mono-objective optimization problem. Hence, a dominant prediction error penalty is a must to ensure a reasonable trajectory prediction, which makes the predictive control loss $J(\cdot,\cdot)$ numerically less relevant. To better see this issue, one can check the feasibility of the predictive scheme (3), where we can assume $\mathbf{0}$ is a feasible point in both $\mathcal{U}$ and $\mathcal{Y}$. The predictive control problem is then always feasible by taking $g = \mathbf{0}$, regardless of y_{init} and u_{init}. This issue is the ultimate cause motivating this work, where we decouple the prediction and the control decision into a bi-level structure.

A. Wasserstein Distance

The 2-Wasserstein distance between two distributions $\mathbb{P}_x$ and $\mathbb{P}_y$ is defined by

$$W(\mathbb{P}_x, \mathbb{P}_y) := \left(\inf_{\gamma \in \Gamma(\mathbb{P}_x, \mathbb{P}_y)} \mathbb{E}_{(x,y)\sim\gamma} \|x-y\|^2 \right)^{\frac{1}{2}} ,$$

where $\Gamma(\mathbb{P}_x, \mathbb{P}_y)$ is the family of joint distributions whose marginals are $\mathbb{P}_x$ and $\mathbb{P}_y$. The 2-Wasserstein distance models the optimal transport between $\mathbb{P}_x$ and $\mathbb{P}_y$ in terms of the Euclidean distance. If $\mathbb{P}_x \sim \mathcal{N}(\mu_x, \Sigma_x)$ and $\mathbb{P}_y \sim \mathcal{N}(\mu_y, \Sigma_y)$, then the squared 2-Wasserstein distance has a closed-form [21]

$$W(\mathbb{P}_x, \mathbb{P}_y)^2 = \|\mu_x - \mu_y\|^2 + \mathrm{tr}\left(\Sigma_x + \Sigma_y - 2(\Sigma_x\Sigma_y)^{\frac{1}{2}}\right) . \tag{4}$$

B. Setting the Stage

In this paper, we focus on the following uncertain time-varying linear system

$$\begin{aligned} x_{i+1} &= A_i x_i + B_i u_i + E_i w_i \\ \overline{y}_i &= C_i x_i + D_i u_i \\ y_i &= \overline{y}_i + v_i \end{aligned} \tag{5}$$

where $w_i \in \mathbb{R}^{n_w}$ is a bounded measurable process noise and $v_i \sim \mathcal{N}(0, \Sigma_v)$ with $v_i \in \mathbb{R}^{n_y}$ an i.i.d unknown measurement noise. In particular, $\overline{y}$ is the system output, which is unknown, and y is the measurement read out from the sensors. In particular, in the building control problem, w mostly reflects the external temperature, solar radiation, occupancy, etc. In a similar manner to [30], [31], by viewing w as uncontrolled inputs, Lemma 1 can be generalized and the corresponding L-step trajectory is augmented to

$$[u_{1:L}, w_{1:L}, y_{1:L}] := [u_1^\top, \dots, u_L^\top, w_1^\top, \dots, w_L^\top, y_1^\top, \dots, y_L^\top]^\top .$$

The trajectory prediction in (3b) is modified accordingly as

$$\begin{bmatrix} \mathfrak{H}_{L,init}(y_{\mathbf{d}}) \\ \mathfrak{H}_{L,init}(u_{\mathbf{d}}) \\ \mathfrak{H}_{L,init}(w_{\mathbf{d}}) \\ \mathfrak{H}_{L,pred}(u_{\mathbf{d}}) \\ \mathfrak{H}_{L,pred}(w_{\mathbf{d}}) \\ \mathfrak{H}_{L,pred}(y_{\mathbf{d}}) \end{bmatrix} g = \begin{bmatrix} y_{init} + \sigma \\ u_{init} \\ w_{init} \\ u_{pred} \\ w_{pred} \\ y_{pred} \end{bmatrix} , \tag{6}$$

whose components follow a similar definition to that in (3b).

III. Robust Bi-level Data-driven Control for LTI Systems

In this part, we will establish a rigorous mathematical framework for our proposed method by considering the LTI version of the targeted time-varying dynamics (5):

$$\begin{aligned} x_{i+1} &= Ax_i + Bu_i + Ew_i \\ \overline{y}_i &= Cx_i + Du_i \\ y_i &= \overline{y}_i + v_i \end{aligned} \tag{7}$$

A Wasserstein distance upper bound between a trajectory given by the fundamental lemma and noisy measurement sequences is summarized in Lemma 2 for LTI systems. The minimization of this upper bound is used to generate a trajectory prediction, which enables a robust data-driven controller for the LTI system in Section III-B. A tractable version of the proposed scheme is discussed in Section III-B, whose single level reformulation is summarized in Lemma 3. The further generalization to time-varying dynamics (5) will be introduced in the next Section IV.

A. Wasserstein Prediction Upper Bound

Regarding (7), the system output $\overline{y}_{init}$ is contaminated by measurement noise, giving a noisy measurement vector y_{init}. The posterior estimate of output $\overline{y}_{init}$ thus follows the distribution:

$$\overline{y}_{init} \sim \mathcal{N}(y_{init}, \Sigma_{init}) ,$$

where $\Sigma_{init} = I_{t_{init}} \otimes \Sigma_v$. Similarly, the measurement Hankel matrix $\mathfrak{H}_{L,init}(y_{\mathbf{d}})$ is subject to measurement noise, and we denote the uncertain posterior estimate of the system output Hankel matrix by $\mathfrak{H}_{L,init}(\overline{y_{\mathbf{d}}})$. Then, for arbitrary $g \in \mathbb{R}^{n_c}$, the following lemma quantifies the distribution distance between an uncertain trajectory generated by the fundamental lemma, $\mathfrak{H}_{L,init}(\overline{y}_{\mathbf{d}})g$, and the uncertain system output sequence $\overline{y}_{init}$

Lemma 2: $\forall\ g \in \mathbb{R}^{n_c}$, the squared Wasserstein distance $W(\mathfrak{H}_{L,init}(\overline{y_{\mathbf{d}}})\, g, \overline{y}_{init})^2$ is upper bounded by

$$\|\mathfrak{H}_{L,init}(y_{\mathbf{d}})g - y_{init}\|^2 + \left(\sqrt{t_{init}}\|g\| - 1\right)^2 \mathrm{tr}(\Sigma_v)\ .$$

Proof: Similar to the posterior distribution of $\overline{y}_{init}$, the posterior distribution of the i-th column of the output Hankel matrix $\mathfrak{H}_{L,init}(\overline{y})$ follows a Gaussian distribution $\mathcal{N}(y_{\mathbf{d},i:i+t_{init}-1}, \Sigma_{init})$ and the adjacent columns are correlated. By the basic properties of Gaussian distributions, we have

$$\mathfrak{H}_{L,init}(\overline{y_{\mathbf{d}}})g \sim \mathcal{N}(\mathfrak{H}_{L,init}(y_{\mathbf{d}})g, \tilde{\Sigma}_{init})\ ,$$

where $\tilde{\Sigma}_{init} = \tilde{G} \otimes \Sigma_v$ and the entry of $\tilde{G} \in \mathbb{R}^{t_{init} \times t_{init}}$ is

$$\tilde{G}_{i,j} = \sum_{n=1}^{n_c - |i-j|} g_n g_{n+|i-j|}\ .$$

Hence, the squared Wasserstein distance $W(\mathfrak{H}_{L,init}(\overline{y_{\mathbf{d}}})g, \overline{y}_{init})^2$ is

$$W(\mathfrak{H}_{L,init}(\overline{y_{\mathbf{d}}})g, \overline{y}_{init})^2 = \|\mathfrak{H}_{L,init}(y_{\mathbf{d}})g - y_{init}\|^2 + \underbrace{\mathrm{tr}(\tilde{\Sigma}_{init} + \Sigma_{init} - 2(\tilde{\Sigma}_{init}\Sigma_{init})^{\frac{1}{2}})}_{(a)}\ .$$

In the rest of the proof, we will upper bound the term (a) above,

$$\begin{aligned}
(a) &= \mathrm{tr}(\tilde{\Sigma}_{init}) + \mathrm{tr}(\Sigma_{init}) + 2\,\mathrm{tr}\left((\tilde{\Sigma}_{init}\Sigma_{init})^{\frac{1}{2}}\right) \\
&= \left(\mathrm{tr}(\tilde{G}) + \mathrm{tr}(I_{t_{init}})\right)\mathrm{tr}(\Sigma_v) - 2\underbrace{\mathrm{tr}\left(\left((\tilde{G}I_{t_{init}}) \otimes \Sigma_v^2\right)^{\frac{1}{2}}\right)}_{(b)} \\
&= t_{init}(\|g\|^2 + 1)\,\mathrm{tr}(\Sigma_v) - 2\underbrace{\mathrm{tr}(\tilde{G}^{\frac{1}{2}} \otimes \Sigma_v)}_{(c)} \\
&= \left(t_{init}(\|g\|^2 + 1) - 2\,\mathrm{tr}(\tilde{G}^{\frac{1}{2}})\right)\mathrm{tr}(\Sigma_v) \\
&\overset{(d)}{\leq} \left(t_{init}(\|g\|^2 + 1) - 2\,\mathrm{tr}(\tilde{G})^{\frac{1}{2}}\right)\mathrm{tr}(\Sigma_v) \\
&= \left(t_{init}(\|g\|^2 + 1) - 2\sqrt{t_{init}}\|g\|\right)\mathrm{tr}(\Sigma_v) \\
&\overset{(e)}{\leq} \left(\sqrt{t_{init}}\|g\| - 1\right)^2 \mathrm{tr}(\Sigma_v)\ ,
\end{aligned} \tag{8}$$

where terms (b) and (c) follow the same fact that $(A \otimes B)(C \otimes D) = AC \otimes BD$. The inequality (d) follows [40, Theorem 1 (ii)]

$$\mathrm{tr}(\tilde{G})^{\frac{1}{2}} \leq \mathrm{tr}(\tilde{G}^{\frac{1}{2}})\ .$$

The inequality (e) uses the fact that $t_{init} \geq 1$. We conclude the proof with

$$W(\mathfrak{H}_{L,init}(\overline{y_{\mathbf{d}}})\, g, \overline{y}_{init})^2 \leq \|\mathfrak{H}_{L,init}(y_{\mathbf{d}})g - y_{init}\|^2 + \left(\sqrt{t_{init}}\|g\| - 1\right)^2 \mathrm{tr}(\Sigma_v)\ .$$

■

Based on the upper bound in Lemma 2, we can generate a trajectory prediction via the following optimization problem:

$$y_{pred} = \mathfrak{H}_{L,pred}(y_{\mathbf{d}})g(w_{pred}) \tag{9a}$$

$$\begin{aligned}
g(w_{pred}) \in \arg\min_{g_l, \sigma_l}\ & \frac{1}{2}\|\sigma_l\|^2 + \left(\sqrt{t_{init}}\|g_l\| - 1\right)^2 \mathrm{tr}(\Sigma_v) \\
\text{s.t.}\ & \begin{bmatrix} \mathfrak{H}_{L,init}(y_{\mathbf{d}}) \\ \mathfrak{H}_{L,init}(u_{\mathbf{d}}) \\ \mathfrak{H}_{L,init}(w_{\mathbf{d}}) \\ \mathfrak{H}_{L,pred}(u_{\mathbf{d}}) \\ \mathfrak{H}_{L,pred}(w_{\mathbf{d}}) \end{bmatrix} g_l = \begin{bmatrix} y_{init} + \sigma_l \\ u_{init} \\ w_{init} \\ u_{pred} \\ w_{pred} \end{bmatrix}\ .
\end{aligned} \tag{9b}$$

The left-hand-side of (9b) gives a trajectory generated by the fundamental lemma, while the right-hand-side of (9b), $[y_{init}^\top, u_{init}^\top, w_{init}^\top, u_{pred}^\top, w_{pred}^\top]^\top$, is the trajectory composed by measurements read out from the sensors, the planned future input and a predicted disturbance trajectory. Thus, optimization problem (9) minimizes the discrepancy upper bound between the posterior estimate of an I/O sequence and an I/O trajectory estimated by the fundamental lemma.

Remark 1: Note that the Hankel matrix $\mathfrak{H}_{L,pred}(y_{\mathbf{d}})$ is also subject to measurement noise (v in (5)), which means that the posterior estimate of a fundamental lemma based predictive trajectory $\mathfrak{H}_{L,pred}(\overline{y}_{\mathbf{d}})g$ is also uncertain and Gaussian with expectation $\mathfrak{H}_{L,pred}(y_{\mathbf{d}})g$. The prediction given by (9a) can therefore be considered as a certainty equivalent prediction. Meanwhile, even though it is possible to consider the uncertainty of y_{pred}, for the sake of a clean layout, we only use the certainty equivalence prediction (9) in this paper.

Remark 2: Different from our analysis, [17] also applies the Wasserstein distance to show that the regularization (term (a) in (3)) minimizes the convex cost $J(\cdot,\cdot)$ with a distributionally robust guarantee. Their result relies on [24] with a less realistic assumption that the rows of the Hankel matrix are i.i.d. However, the rows of inputs and the rows of outputs may fail to be independently distributed as they should be linearly correlated by the system dynamics.

B. Tractable Bi-level Formulation for LTI systems

We hope to maintain the system performance while ensuring robust constraint satisfaction regardless of future realizations of the process noise, and so we assume that the future process noise w_{pred} can be predicted with uncertainty quantification. Buildings are systems satisfying this assumption. For example, the weather forecast can provide a future temperature prediction with an uncertainty tube centered around a nominal prediction, such that the actual future temperature realization fluctuates within this tube. Therefore, we denote the set of predicted future process noise realizations by

$$w_{pred} \in \overline{w} \oplus \mathcal{W}\ ,$$

where $\overline{w}$ is the nominal prediction and $\mathcal{W}$ denotes the uncertainty tube. And we state our assumption:

Assumption 1: $\overline{w}$ and $\mathcal{W}$ are known.

To make the controller less conservative, we consider a predictive control input with a linear feedback from process

noise

$$u_{pred} = \overline{u}_{pred} + K w_{pred} \,, \tag{10}$$

where the feedback control K is a decision variable in our predictive control problem. In particular, $\overline{u}$ reflects the nominal control inputs while feedback K adapts the control input based on the actual realization of the process noise.

Based on the prediction problem (9), we can state a bi-level robust predictive control problem for LTI systems:

$$\begin{aligned}
\min_{\substack{\overline{y}_{pred} \\ \overline{u}_{pred}, K}} \quad & J(y_{pred}, u_{pred}) \qquad (11)\\
\text{s.t. } \forall\, & w_{pred} \in \overline{w} \oplus \mathcal{W} \\
& u_{pred} = \overline{u}_{pred} + K w_{pred} \in \mathcal{U} \,, \\
& y_{pred} = \mathfrak{H}_{L,pred}(y_{\mathbf{d}}) g(w_{pred}) \in \mathcal{Y} \,, \\
& g(w_{pred}) \in \arg\min_{g_l, \sigma_l} \frac{1}{2}\|\sigma_l\|^2 + \left(\sqrt{t_{init}}\|g_l\| - 1\right)^2 \operatorname{tr}(\Sigma_v) \\
& \text{s.t.} \begin{bmatrix} \mathfrak{H}_{L,init}(y_{\mathbf{d}}) \\ \mathfrak{H}_{L,init}(u_{\mathbf{d}}) \\ \mathfrak{H}_{L,init}(w_{\mathbf{d}}) \\ \mathfrak{H}_{L,pred}(u_{\mathbf{d}}) \\ \mathfrak{H}_{L,pred}(w_{\mathbf{d}}) \end{bmatrix} g_l = \begin{bmatrix} y_{init} + \sigma_l \\ u_{init} \\ w_{init} \\ u_{pred} \\ w_{pred} \end{bmatrix} .
\end{aligned}$$

The upper level problem sends $\overline{u}_{pred}$ and the feedback control law K to the lower level problem, the lower level problem returns the corresponding set of predictors $g(w_{pred})$ with respect to a given w_{pred}, which accordingly gives the output trajectory predictions y_{pred} for that w_{pred}. In turn, the robust constraint in the upper level ensures that input and output constraints are satisfied for all w_{pred} in the considered set $\overline{w} \oplus \mathcal{W}$. In conclusion, the upper level problem optimizes $\overline{u}_{pred}$ and K based on the prediction given by the lower level problem.

The bi-level problem (11) is hard to solve numerically, because the objective in the lower level problem is non-convex.[1] To address this issue, we state a looser, but convex, Wasserstein upper bound in the following corollary.

Corollary 1: $\forall\, g \in \mathbb{R}^{n_c}$, the squared Wasserstein distance $W(\mathfrak{H}_{L,init}(\overline{y_{\mathbf{d}}})\, g, \overline{y}_{init})^2$ is upper bounded by

$$\|\mathfrak{H}_{L,init}(y_{\mathbf{d}}) g - y_{init}\|^2 + t_{init} \operatorname{tr}(\Sigma_v) \left(\|g\|^2 + 1\right).$$

Proof: In the inequality (d) of Equation (8), we have $\operatorname{tr}(\tilde{G}) \geq 0$ as $\tilde{G}$ is positive semi-definite. Therefore, we give a convex Wasserstein distance upper bound as

$$\begin{aligned}
& W\left(\mathfrak{H}_{L,init}(\overline{y_{\mathbf{d}}})\, g, \overline{y}_{init}\right)^2 \\
& \quad \leq \|\mathfrak{H}_{L,init}(y_{\mathbf{d}}) g - y_{init}\|^2 + t_{init}^2 \operatorname{tr}(\Sigma_v) \left(\|g\|^2 + 1\right) .
\end{aligned}$$

■

Bringing everything together, we have a numerically tractable robust data-driven predictive control problem for LTI systems:

$$\begin{aligned}
\min_{\substack{\overline{y}_{pred} \\ \overline{u}_{pred}, K}} \quad & J(y_{pred}, u_{pred}) \\
\text{s.t. } \forall\, & w_{pred} \in \overline{w} \oplus \mathcal{W} \\
& u_{pred} = \overline{u}_{pred} + K w_{pred} \in \mathcal{U} \,, \\
& y_{pred} = \mathfrak{H}_{L,pred}(y_{\mathbf{d}}) g(w_{pred}) \in \mathcal{Y} \,, \\
& g(w_{pred}) \in \arg\min_{g_l, \sigma_l} \frac{1}{2}\|\sigma_l\|^2 + g_l^\top \mathcal{E}_g g_l \qquad (12a)\\
& \text{s.t.} \begin{bmatrix} \mathfrak{H}_{L,init}(y_{\mathbf{d}}) \\ \mathfrak{H}_{L,init}(u_{\mathbf{d}}) \\ \mathfrak{H}_{L,init}(w_{\mathbf{d}}) \\ \mathfrak{H}_{L,pred}(u_{\mathbf{d}}) \\ \mathfrak{H}_{L,pred}(w_{\mathbf{d}}) \end{bmatrix} g_l = \begin{bmatrix} y_{init} + \sigma_l \\ u_{init} \\ w_{init} \\ u_{pred} \\ w_{pred} \end{bmatrix} ,
\end{aligned}$$

where $\mathcal{E}_g = t_{init}^2 \operatorname{tr}(\Sigma_v) I_{n_c}$ and the lower level problem drops the constant term $t_{init}^2 \operatorname{tr}(\Sigma_v)$ in its objective for the sake of clarity. The main benefit of the proposed predictive control problem (12) is that it resolves the issue discussed in Section II by decoupling the trajectory prediction from control decision-making into a bi-level optimization problem, which guarantees that the control is chosen with a reliable trajectory prediction.

To derive a tractable single level problem, we denote

$$H := \begin{bmatrix} \mathfrak{H}_{L,init}(u_{\mathbf{d}}) \\ \mathfrak{H}_{L,init}(w_{\mathbf{d}}) \\ \mathfrak{H}_{L,pred}(u_{\mathbf{d}}) \\ \mathfrak{H}_{L,pred}(w_{\mathbf{d}}) \end{bmatrix} .$$

The bi-level problem (12) can be effectively solved via the following reformulation.

Lemma 3: The following single-level robust optimization problem is equivalent to the bi-level problem (15).

$$\begin{aligned}
\min_{\substack{\overline{y}_{pred} \\ \overline{u}_{pred}, K}} \quad & J(y_{pred}, u_{pred}) \\
\text{s.t. } \forall\, & w_{pred} \in \overline{w} \oplus \mathcal{W} \\
& u_{pred} = \overline{u}_{pred} + K w_{pred} \in \mathcal{U} \,, \\
& y_{pred} = \mathfrak{H}_{L,pred}(y_{\mathbf{d}}) g(w_{pred}) \in \mathcal{Y} \,, \\
& \begin{bmatrix} g(w_{pred}) \\ \kappa \end{bmatrix} = M^{-1} \begin{bmatrix} \mathfrak{H}_{L,init}(y_{\mathbf{d}})^\top y_{init} \\ u_{init} \\ w_{init} \\ u_{pred} \\ w_{pred} \end{bmatrix} , \qquad (13a)
\end{aligned}$$

where

$$M = \begin{bmatrix} \mathfrak{H}_{L,init}^\top(y_{\mathbf{d}})\, \mathfrak{H}_{L,init}(y_{\mathbf{d}}) + \mathcal{E}_g & H^\top \\ H & \mathbf{O} \end{bmatrix} .$$

Proof: Note that the uncertain lower level problem in (15) is strongly convex and therefore can be equivalently represented by its KKT system [19, Chapter 4]. By replacing σ_l by $\mathfrak{H}_{L,init}(y_{\mathbf{d}}) g_l - y_{init}$, the Lagrangian of the lower-level

[1] To ensure a composition of two convex functions is convex, the outer convex function needs be non-decreasing [13, Chapter 3.2.4]. To see the non-convexity in (11), one can plot the following function $f(x) = (|x|-1)^2, x \in \mathbb{R}$.

problem is

$$\mathcal{L}(g) = \frac{1}{2}\|\mathfrak{H}_{L,init}(y_{\mathbf{d}})g_l - y_{init}\|^2 + \frac{1}{2}g^\top \mathcal{E}_g g + \kappa^\top (Hg - \begin{bmatrix} u_{init} \\ w_{init} \\ u_{pred} \\ w_{pred} \end{bmatrix}) ,$$

where κ is the dual variable of the equality constraint. Based on this, we have the stationary condition of the KKT system

$$\frac{\partial \mathcal{L}(g)}{g} = (\mathfrak{H}_{L,init}(y_{\mathbf{d}})^\top \mathfrak{H}_{L,init}(y_{\mathbf{g}}) + \mathcal{E}_g)g + H^\top \kappa - \mathfrak{H}_{L,init}(y_{\mathbf{d}})^\top y_{init} = 0 .$$

By recalling the primal feasibility condition

$$Hg = \begin{bmatrix} u_{init} \\ w_{init} \\ u_{pred} \\ w_{pred} \end{bmatrix} ,$$

we get the uncertain KKT equation in (13a), which concludes the proof. ■

On top of the single-level problem (13), we further enforce causality on the decision variable K through a lower-block triangular structure [33, Chapter 5.1],

$$K = \begin{bmatrix} \mathbf{O} & \mathbf{O} & \mathbf{O} & \dots & \vdots \\ K_{2,1} & \mathbf{O} & \mathbf{O} & \dots & \vdots \\ K_{3,1} & K_{3,2} & \mathbf{O} & \dots & \vdots \\ \vdots & \ddots & \ddots & \ddots & \vdots \\ K_{n_h,1} & K_{n_h,2} & K_{n_h,3} & \dots & \mathbf{O} \end{bmatrix} . \tag{14}$$

In particular, causality means that the i-th step of the future process noise can only change the events happening later than it, which only includes $u_{pred,i+1:n_h}$.

Remark 3: When the feasible sets $\mathcal{U}, \mathcal{Y}$ are polytopic, the robust optimization problem (13) can be solved by a standard dualization procedure [6].

Remark 4: The single level problem stated in Lemma 3 uses an optimality condition to generate trajectory prediction. A similar idea is applied in subspace predictive control [26], which identifies an ARX model online. These two methods are different: the analysis carried out in subspace predictive control falls into the category of the least square analysis of over-determined linear equations [29], which particularly assumes that $\mathfrak{H}_{L,init}(y_{\mathbf{d}})$ is noise-free [28]. The proposed controller does not have this assumption, and the lower level problem in (15) can also optimize an under-determined equation system.

IV. Heuristic Time-varying Extension

In this section, we will generalize the controller (12) to time-varying dynamics (5) heuristically. We first summarize the optimization problem solved in our novel adaptive robust controller, whose details will be elaborated later accordingly.

The following optimal control problem will optimize the u_{pred} and the feedback K under a receding horizon scheme,

$$\begin{aligned} \min_{\substack{\overline{y}_{pred} \\ \overline{u}_{pred}, K}} \quad & J(y_{pred}, u_{pred}) \\ \text{s.t. } & \forall\, \tilde{w}_{pred} \in \tilde{\mathcal{W}} && \text{(15a)} \\ & u_{pred} = \overline{u}_{pred} + K\tilde{w}_{pred} \in \tilde{\mathcal{U}} , && \text{(15b)} \\ & y_{pred} = \mathfrak{H}_{L,pred}(y_{\mathbf{d}})g \in \mathcal{Y} , && \text{(15c)} \\ & g \in \arg\min_{g_l, \sigma_l} \frac{1}{2}\|\sigma_l\|^2 + \frac{1}{2} g_l^\top \mathcal{E}_g g_l \\ & \text{s.t.} \begin{bmatrix} \mathfrak{H}_{L,init}(y_{\mathbf{d}}) \\ \mathfrak{H}_{L,init}(u_{\mathbf{d}}) \\ \mathfrak{H}_{L,init}(\tilde{w}_{\mathbf{d}}) \\ \mathfrak{H}_{L,pred}(u_{\mathbf{d}}) \\ \mathfrak{H}_{L,pred}(\tilde{w}_{\mathbf{d}}) \end{bmatrix} g_l = \begin{bmatrix} y_{init} + \sigma_l \\ u_{init} \\ \tilde{w}_{init} \\ u_{pred} \\ \tilde{w}_{pred} \end{bmatrix} , \end{aligned}$$

where $\mathcal{E}_g$ is replaced by a diagonal matrix $\text{diag}(\eta_{g,1}, \dots, \eta_{g,n_c})$ and the weight sequence $\{\eta_{g,i}\}_{i=1}^{n_c}$ is decreasing. The feasible set of control input $\tilde{\mathcal{U}}$ in (15b), the perturbation $\tilde{w}$, and the uncertainty set $\tilde{\mathcal{W}}$ in (15a) are determined by the working mode, whose details will be given in Section IV-A.

In general, we apply two heuristics to adapt the LTI controller in (12) to the time-varying dynamics (5). The modifications are summarized as follows:

- **Modification of the lower level objective:** Note that the objective function in the lower level problem in (12) consists of a penalty on $\|\sigma\|^2$ and a penalty on $\|g\|^2$. Recall that the i-th entry of g, g_i, is the weight of the i-th column in H and $\mathfrak{H}_{L,init}(y_{\mathbf{d}})$ used for prediction. Thus, an inhomogeneous penalty on g can be used to model our preference of using recent data for trajectory prediction, and the decreasing diagonal elements in $\mathcal{E}_g$ reflect this preference.
- **Adaptation of the measured dataset:** The data are updated online to capture the latest dynamics from the system. In particular, Hankel matrices are updated by appending new input/output measurements on the right side of the Hankel matrices and by discarding old data on the left side.

Remark 5: The single-level reformulation in Lemma 3 can be applied in this adaptive problem by replacing H with

$$H = \begin{bmatrix} \mathfrak{H}_{L,init}(u_{\mathbf{d}}) \\ \mathfrak{H}_{L,init}(\tilde{w}_{\mathbf{d}}) \\ \mathfrak{H}_{L,pred}(u_{\mathbf{d}}) \\ \mathfrak{H}_{L,pred}(\tilde{w}_{\mathbf{d}}) \end{bmatrix} .$$

A. Active Excitation

In this part, we will discuss the selection of the $\tilde{\mathcal{U}}$ and $\tilde{\mathcal{W}}$ in (13). Recall that persistent excitation is the key assumption required for Willems' fundamental lemma to apply. However, the update of Hankel matrices may cause a loss of persistent excitation as it is not explicitly considered in the predictive control problem (13). For example, in building control, if the outdoor temperature and/or solar irradiation are near the building's equilibrium point, no extra heating/cooling is needed if

the controller is designed to minimize energy consumption. In this case, the control input will be 0 for a long time, leading to a loss of persistent excitation. To accommodate this issue, we introduce a robust active excitation scheme, which perturbs the control input applied at time i by a random excitation signal

$$u_i = \underbrace{\overline{u}_{pred,1|i}}_{(a)} + \underbrace{u_{e,i}}_{(b)}, \tag{16}$$

where $\overline{u}_{pred,1|i}$ is the first element of $\overline{u}_{pred}$ determined by a predictive control problem (13) solved at time i. In this decomposition, term (a) is determined by the predictive control problem (13) with some specific choice of $\tilde{\mathcal{U}}$ and $\tilde{\mathcal{W}}$ (see Algorithm (1) below), and the term (b) is a bounded excitation input, which is unknown to the decision process of $\overline{u}_{pred,1|i}$. More specifically, from the viewpoint of u_{pred}, u_e is an uncontrolled, but measurable, process noise and the underlying time-varying process dynamics therefore becomes

$$x_{i+1} = A_i x_i + B_i u_{pred,1|i} + [E_i, B_i] \begin{bmatrix} w_i \\ u_{e,i} \end{bmatrix},$$

where the excitation input is randomly sampled from a user-defined compact set as $u_e \in \mathcal{U}_e \subset \mathcal{U}$. The process noise $\tilde{w}$ is accordingly augmented to $[w_{pred}^\top, u_e^\top]^\top$, and the uncertainty set $\tilde{\mathcal{W}}$ in (15a) is augmented to $(\overline{w} \oplus \mathcal{W}) \times \mathcal{U}_e$. Meanwhile, due to an extra excitation signal in (16), the feasible set of the control input $\tilde{\mathcal{U}}$ is tightened to $\mathcal{U} \ominus \mathcal{U}_e$.

In practice, this active excitation mechanism sacrifices the flexibility of the control input for data quality. If not necessary, we should set $\tilde{\mathcal{U}} = \mathcal{U}$ and $\tilde{\mathcal{W}} = \mathcal{W}$ to generate control inputs instead of using the active excitation scheme. We summarize the general algorithm of the proposed controller in Algorithm 1, which automatically selects the uncertainty set $\tilde{\mathcal{W}}$ and input feasible set $\tilde{\mathcal{U}}$.

Algorithm 1

while true **do**
  Measure y_i, w_i and update Hankel matrices.
  $\tilde{\mathcal{U}} \leftarrow \mathcal{U}, \tilde{\mathcal{W}} \leftarrow \overline{w} \oplus \mathcal{W}$
  Solve problem (13) to get $\overline{u}_{pred|i}$
  if $\{u_{\mathbf{d}}, \overline{u}_{pred|i}\}$ loose persistent excitation **then**
    $\tilde{\mathcal{U}} \leftarrow \mathcal{U} \ominus \mathcal{U}_e$, $\tilde{\mathcal{W}} \leftarrow (\overline{w} \oplus \mathcal{W}) \times \mathcal{U}_e$
    Solve problem (13) to get $\overline{u}_{pred|i}$
    Sample $u_{e,i}$ from $\mathcal{U}_e$
    Apply $u_i = \overline{u}_{pred,1|i} + u_{e,i}$
  else
    Apply $u_i = \overline{u}_{pred,1|i}$
  end if
  $i \leftarrow i + 1$
end while

In this algorithm, the problem (13) is first solved without active excitation. If its solution expects a loss of persistent excitation, the problem (13) is re-solved considering the active excitation. If checking the satisfaction of persistent excitation by the rank condition results in too high a computational cost, this condition can be replaced by other heuristic conditions. In building control, loss of persistent excitation mainly happens when the control input is constant, and thus the persistence excitation condition can be replaced by checking whether the nominal input is a constant sequence.

Remark 6: In general, generating a persistently excited control input while considering control performance is challenging, as the persistent excitation condition depends on the rank of $\mathfrak{H}_L(u_{\mathbf{d}})$, which turns the optimization problem into a challenging non-smooth non-convex optimization [35]. It is noteworthy that [25] also perturbs the nominal control input to guarantee persistent excitation, however, their result has no guarantee of robust constraint satisfaction.

Remark 7: Due to the causality constraints in (14), the matrix K in (15b) cannot instantaneously counteract the excitation signal u_e with a $K = [K_w, -I]$, which is non-causal.

B. Numerical Details

In our proposed adaptive robust controller, the Hankel matrices are updated online with the real-time measurement of u_i, y_i, w_i (Section IV and Algorithm 1). Meanwhile, a numerically efficient reformulation of the robust problem (13) requires an explicit evaluation of matrix inversion M^{-1} in (13a) at each update. More specifically, when the feasible sets $\tilde{\mathcal{U}}, \mathcal{Y}$ and the uncertainty set $\tilde{\mathcal{W}}$ are polytopic or ellipsoidal, the dualization/explicit upper bound of the robust inequality constraint depends on the matrix inversion M^{-1}. However, the computational cost of M^{-1} is $O((n_c+n_r)^3)$ [43] with n_r the number of rows in the matrix H, which is roughly cubic in the size of the data set and it is therefore not scalable. Thus, we propose to apply two linear algebraic techniques to resolve this computational bottleneck.

Notice that the dual variable κ in the lower problem does not affect the upper level problem. For the sake of compactness, we denote $M_{1,1} := \mathfrak{H}_{L,init}^\top(y_{\mathbf{d}})\mathfrak{H}_{L,init}(y_{\mathbf{d}}) + \mathcal{E}_g$. By matrix inversion of a block-structured matrix, we have

$$M^{-1} = \begin{bmatrix} M_{1,1}^{-1} - M_{1,1}^{-1}H^\top(HM_{1,1}^{-1}H^\top)^{-1}HM_{1,1}^{-1} & M_{1,1}^{-1}H^\top(HM_{1,1}^{-1}H^\top)^{-1} \\ (HM_{1,1}^{-1}H^\top)^{-1}HM_{1,1}^{-1} & -(HM_{1,1}^{-1}H^\top)^{-1} \end{bmatrix}.$$

We can therefore replace the constraint (13a) by

$$g(w_{pred}) = M_t \begin{bmatrix} \mathfrak{H}_{L,init}(y_{\mathbf{d}})^\top y_{init} \\ u_{init} \\ \tilde{w}_{init} \\ u_{pred} \\ \tilde{w}_{pred} \end{bmatrix},$$

where

$$M_t := \begin{bmatrix} M_{1,1}^{-1} - M_{1,1}^{-1}H^\top(HM_{1,1}^{-1}H^\top)^{-1}HM_{1,1}^{-1} & M_{1,1}^{-1}H^\top(HM_{1,1}^{-1}H^\top)^{-1} \end{bmatrix}.$$

With the aforementioned modification, the computational cost is lowered to $O(n_c^3)$ with only the inversion of $M_{1,1}$. We further lower the computational cost by the Woodbury matrix

identity,

$$\begin{aligned} &M_{1,1}^{-1} \\ &= (\mathfrak{H}_{L,init}^{\top}(y_{\mathfrak{d}})\,\mathfrak{H}_{L,init}(y_{\mathfrak{d}}) + \mathcal{E}_g)^{-1} \\ &= \mathcal{E}_g^{-1} - \mathcal{E}_g^{-1}\,\mathfrak{H}_{L,init}^{\top}(y_{\mathfrak{d}}) \\ &\qquad \underbrace{\left(I_m + \mathfrak{H}_{L,init}(y_{\mathfrak{d}})\mathcal{E}_g^{-1}\,\mathfrak{H}_{L,init}^{\top}(y_{\mathfrak{d}})\right)^{-1}}_{(a)} Han_{L,init}(y_{\mathfrak{d}})\mathcal{E}_g^{-1}. \end{aligned} \tag{17}$$

As $\mathcal{E}_g$ is diagonal with a simple and explicit inversion, the major computation cost happens at the inversion of a size m matrix in term (a), where $m := n_y * t_{init}$. Thus, the computational cost of $M_{1,1}^{-1}$ and M_t is lowered to $O(m^3)$, which is fixed and independent of the number of columns in the Hankel matrices (*i.e.* roughly the size of the data-set).

Remark 8: Note that the KKT matrix is usually ill-conditioned [41, Chapter 16], replacing the full matrix inversion in (13a) with the proposed techniques can improve the numerical stability, because only the matrix inversion of $\mathcal{E}_g$ and the term (a) in (17) are evaluated, and these two matrices are well-conditioned.

V. Numerical Results

In this part, we will first demonstrate that our proposed scheme shows comparable performance against some model-based methods in both LTI and time-varying linear systems.

A. Second-Order System

It should be noted that we are not claiming that the data-driven approach outperforms all model-based approaches, as it is definitely possible to tune a better model based method, such as considering the uncertainty of the identified parameters or using a more complex estimator/controller. We only aim to show that the proposed approach has comparable performance against a model-based method, but without requiring a model. We therefore select a standard model-based controller design pipeline that we believe is reasonable, and we compare this standard scheme against our proposed scheme in this example. The considered second order system is:

$$\begin{aligned} x_{i+1} &= \begin{bmatrix} 0.9535 & 0.0761 \\ -0.8454 & 0.5478 \end{bmatrix} x_i + \begin{bmatrix} 0.0465 \\ 0.8454 \end{bmatrix} u_i + \begin{bmatrix} 0.0465 \\ 0.8454 \end{bmatrix} w_i \,, \\ \overline{y}_i &= \begin{bmatrix} 1 & 0 \end{bmatrix} x_i \\ y_i &= \overline{y}_i + v_i \,, \end{aligned}$$

where the unknown measurement noise v of two different standard deviations are considered to show the reliability of the proposed scheme. We remind the reader that only the measurement y_i is available to both schemes and $\overline{y}_i$ is unknown to both schemes.

In the 'standard' scheme, the model is identified by a subspace identification algorithm and the state estimation is done by a Kalman filter[2]. Following this, a robust model predictive controller with linear feedback [33] is used with the standard procedure to generate control inputs[3]

$$\begin{aligned} \min_{\substack{u_{pred}, K_w \\ y_{pred}}} \max_{w_{pred}} \; & J(y_{pred}, u_{pred}) \\ \text{s.t. } & x_{pred,0} = x_0 \\ & \forall\, i = 0, 1 \ldots, n_h \\ & x_{pred,i+1} = A_{id} x_{pred,i} + B_{id} u_{pred,i} + E_{id} w_{pred,i} \\ & y_{pred,i} = C_{id} x_{pred,i} + D_{id} u_{pred,i} \\ & \forall\, w_{pred} \in \mathcal{W} \;,\; u_{pred} = \overline{u}_{pred} + K_w w_{pred} \\ & u_{pred} \in \mathcal{U} \;,\; y_{pred} \in \mathcal{Y} \;, \end{aligned} \tag{18}$$

where the parameters of A_{id} , B_{id} , E_{id} , C_{id} , D_{id} come from system identification and x_0 is estimated with a Kalman filter. Note that the feedback control law K_w is optimized by (18). Other components, such as $J(\cdot,\cdot)$, n_h and $\mathcal{U}, \mathcal{Y}, \mathcal{W}$, are identical to those used in the proposed robust data-driven scheme. In particular, we use $-10 \leq u_{pred} \leq 10$, $-2 \leq y_{pred} \leq 0.5$ and $-1 \leq w_{pred} \leq 1$. The loss function is

$$J(y_{pred}, u_{pred}) = \sum_{i=0}^{n_h} 10(y_{pred,i+1} - y_{ref})^2 + 0.1 u_{pred,i}^2 \;,$$

where y_{ref} is the tracking reference and the prediction horizon is set to $n_h = 10$. Meanwhile, we set $t_{init} = 4$ in the proposed robust scheme. Finally, to ensure a better model identification result, the standard scheme uses a dataset larger than the one used for the proposed scheme. In particular, 200 data points generated by a PRBS excitation signal is used to identify the model used in (18), while the proposed scheme only used the first 60 points of this dataset.

Measurement noise standard deviation	0.01	0.2
Proposed scheme	0.03%	3.2%
Standard scheme	1.2%	35.9%

TABLE I

AVERAGE CONSTRAINT VIOLATION IN MONTE-CARLO RUNS (*We only consider the 38 steps where the reference signal overlaps the upper bound of the output constraint*)

Two experiments with different levels of measurement noise are considered, whose results are shown in Figure 1[4] and Table I, and each experiment carries out 50 Monte-Carlo runs. In particular, the constraint violation is calculated by

$$\frac{\text{number of steps where a constraint violation occurs}}{(\text{number of simulation steps} \times \text{number of Monte-Carlo runs})} \,.$$

In the test of Figure 1 (a), the standard deviation of the measurement noise is 0.01, which corresponds to a maximal signal to noise ratio of 500 in the data[5]. In this case, the averaged 10-step prediction accuracy[6] of the identified state space model is 99.1%. From Figure 1 (a), we can see that the

[2]We use the commands N4SID and KALMAN in MATLAB to do subspace identification and Kalman filter design respectively

[3]We used the templated code of "Approximate closed-loop minimax solution" in https://yalmip.github.io/example/robustmpc.

[4]To be fair, both controllers are subject to the same measurement noise and process noise during their online operation.

[5]The amplitude of the output y is within $[-5, 5]$, and mainly fluctuates around $[-2, 2]$. Hence, we claim that the signal noise ratio is at most 500, and its actual value should be much lower.

[6]This accuracy is generated by the MATLAB command COMPARE.

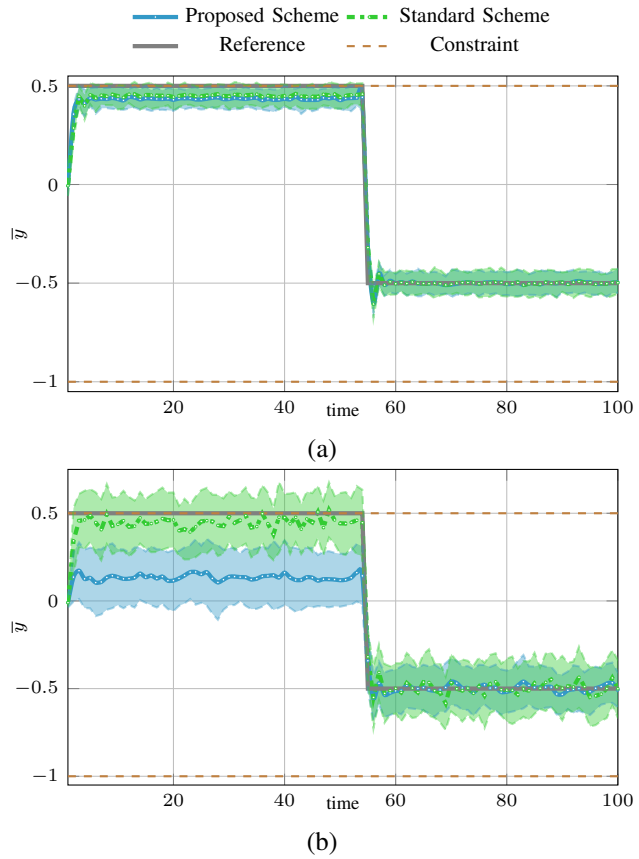

Fig. 1. Comparison of the proposed robust data-driven control and the controller designed by standard procedure. Shaded region is the mean plus/minus the two standard deviation of all Monte-Carlo runs. Standard deviation of measurement noise: (a) 0.01, (b) 0.2

proposed scheme shows comparable performance against the model based scheme. In the test of Figure 1 (b), the standard deviation of the process noise reaches 0.2, leading to a minimal signal to noise ratio of 25. In this case, the averaged 10-step prediction accuracy of the identified state space model is 71.1%. Note that this accuracy is not low because of the large measurement noise, which will still cause a prediction error of roughly 20% even when a perfect model is used. While both controllers violate the constraints more frequently in this case, our proposed scheme offers a better constraint satisfaction guarantee. The constraint violation statistics are summarized in Table I, and we observe that our proposed controller offers much better constraint satisfaction. Meanwhile, due to our discussion in Remark 1, the proposed scheme is certainty equivalent and still also encountered a few constraint violations in both tests.

We believe that the constraint violation in the model-based method is caused by the inaccuracy of the identified model and can be resolved by methods such as constraint tightening, but there is currently no systematic way of achieving this. Finally, it is noteworthy that the measurement noise used in Figure 1(a) is realistic, while the second test in Figure 1(b) is intended to be a stress test of the proposed control scheme, in order to show the robustness of the proposed scheme to unknown measurement noise.

In the second test, we consider the following time-varying system

$$\begin{aligned} x_{i+1} &= A_i x_i + \begin{bmatrix} 0.0465 \\ 0.8454 \end{bmatrix} u_i + \begin{bmatrix} 0.0465 \\ 0.8454 \end{bmatrix} w_i \ , \\ \overline{y}_i &= \begin{bmatrix} 1 & 0 \end{bmatrix} x_i \ , \\ y_i &= \overline{y}_i + v_i \ , \\ A_i &= \begin{bmatrix} 0.9535 + 0.1\sin(\frac{i\pi}{48}) & 0.0761 \\ -0.8454 & 0.5478 + 0.1\sin(\frac{i\pi}{48}) \end{bmatrix} . \end{aligned}$$

Our proposed scheme is compared against a model based adaptive method, where a recursive least square (RLS) estimator updates the parameter of an ARX model:

$$y_i = \sum_{j=1}^{t_{init}} \theta_{y,j} y_{i-j} + \theta_{u,j} u_{i-j} + \theta_{w,j} w_{i-j} \ .$$

The model estimated by RLS is used in the following robust MPC problem:

$$\begin{aligned} \min_{\substack{u_{pred}, K_w \\ y_{pred}}} \ & \max_{w_{pred}} \ J(y_{pred}, u_{pred}) \\ \text{s.t. } & x_{pred,0} = x_0 \\ & \forall\, i = 0, 1 \ldots, n_h \\ & y_{pred,i} = \sum_{j=1}^{t_{init}} \theta_{y,j} y_{pred,i-j} + \theta_{u,j} u_{pred,i-j} + \theta_{w,j} w_{pred,i-j} \\ & \forall\, w_{pred} \in \mathcal{W} \ , \ u_{pred} = \overline{u}_{pred} + K_w w_{pred} \\ & u_{pred} \in \mathcal{U} \ , \ y_{pred} \in \mathcal{Y} \ , \end{aligned} \tag{19}$$

where the parameters θ_y, θ_u and θ_w are updated by the RLS estimator. The other settings are the same as the previous experiment. In particular, the RLS estimator has a forgetting factor of 0.95 and it is initialized by the data used to build the Hankel matrices of the proposed scheme. Two experiments with different levels of measurement noise standard deviation are conducted. The results are shown in Figure 2 and the constraint violation statistics are given in Table II. We can see that both approaches perform the tracking task properly, and the proposed scheme shows comparable performance against the RLS-MPC approach. One major observation is that the proposed scheme shows better constraint satisfaction against the RLS-MPC method. It is possible to consider the uncertainty generated by the RLS estimator to improve the robustness of the model-based approach, however, it turns out to be a non-convex robust optimization problem and there is no standard approach to solve this problem.

Measurement noise standard deviation	0.01	0.1
Proposed scheme	0.09%	0.38%
RLS-MPC scheme	14.8%	20.1%

TABLE II
AVERAGE CONSTRAINT VIOLATION IN MONTE-CARLO RUNS (*We only consider the 38 steps where the reference signal overlaps the upper bound of the output constraint*)

VI. EXPERIMENT

This part presents our real-world experiments conducted at a conference building on the EPFL campus.

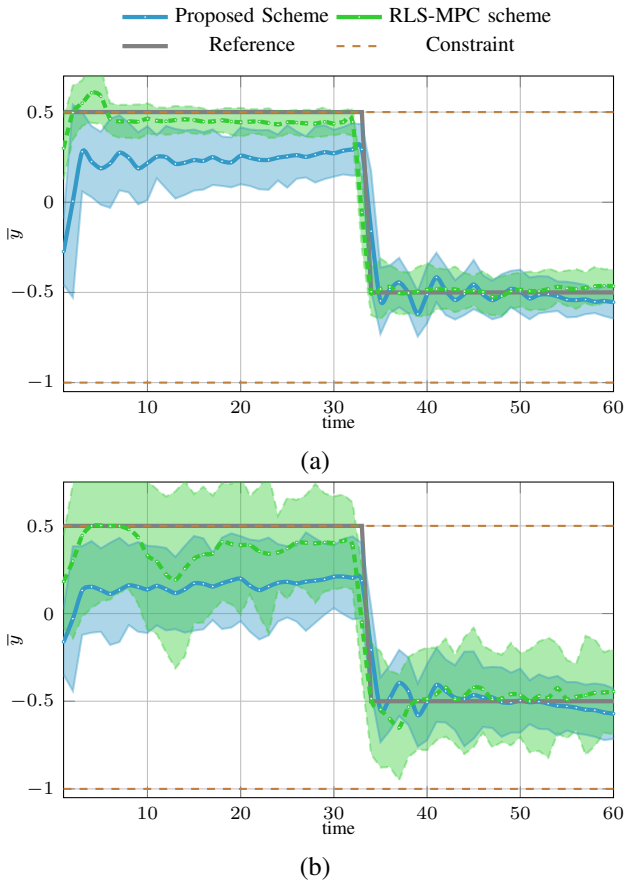

Fig. 2. Comparison of the proposed robust data-driven control and controller designed by RLS and robust MPC procedure. The shaded region is the mean plus/minus the two standard deviation of all Monte-Carlo runs. Standard deviation of measurement noise: (a) 0.01, (b) 0.1

A. Experimental Setup

The building control experiment is conducted on an entire building, which is a freestanding $600m^2$ single-zone building on the EPFL campus, called the *Polydome*. It is regularly used for lectures/exams and accommodates up to 200 people (Figure 3).

Fig. 3. The Polydome

In the presented experiments, the indoor temperature is the output y, the active electrical power consumption of the HVAC system is the input u, and the weather conditions (outdoor temperature and solar radiation) are the process noise $w = [w_1; w_2]$. The sampling period is 15 minutes and the structure of the control system is depicted in Figure 4, where the arrows indicate the direction of data transmission. The system consists of five main components

- **Sensors**: Four Z-wave FIBARO DOOR/WINDOW SENSOR v2 are put in different locations in the *Polydome* to measure the indoor temperature (path (a)). Every five minutes, the temperature measurements are sent to the database through a wireless Z-wave network (path (c)). The average value of the four measurements is used as the indoor temperature. The active power consumption of the HVAC system is measured via an EMU 3-phase power meter [1] (path (b)).
- **Database**: We use INFLUXDB 1.3.7 [2] to log the time-series data, which records the measurements from sensors (path (c)), the control input computed from the PC (path (d)) and the historical weather (path (f)).
- **Weather API**: We use TOMORROW.IO [3], which provides both historical and current measurements of solar radiation and outdoor temperature to the database (path (f)). It also provides the forecast of solar radiation and outdoor temperature to the PC to solve the predictive control problem (path (g)).
- **Controller**: The controller is implemented in MATLAB, interfacing YALMIP, which fetches historical data from the database to build/update the Hankel matrices (path (d)), and acquires weather forecasts from the weather API (path (g)). It runs Algorithm 1 to generate the control input. This control signal is transmitted to the HVAC system via the serial communication protocol, Modbus [45].
- **HVAC**: A roof-top HVAC unit (series No: AERMEC RTY-04 heat pump) is used for heating, cooling and ventilation. Its heating and cooling units are different, consisting of two compressors for heating and one compressor for cooling respectively.

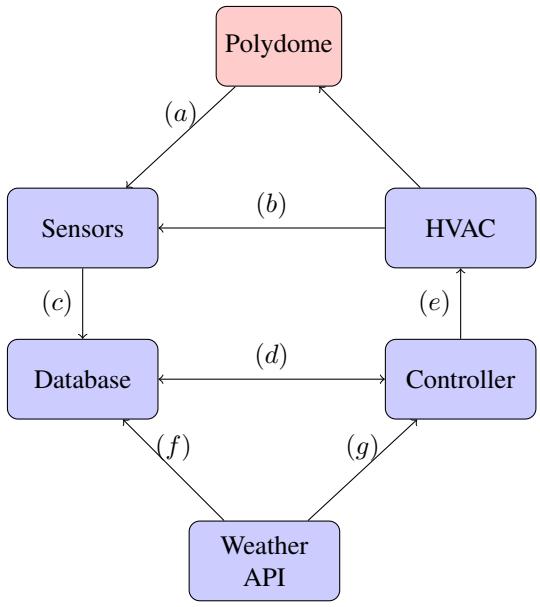

Fig. 4. Structure of the building control system

The HVAC system is shipped with an internal hierarchical controller, which includes:

- **Mode scheduler:** The scheduler determines whether the HVAC is in heating or cooling mode, and we are **not** authorized to access this scheduler.
- **Temperature controller:** The indoor temperature is controlled by a bang-bang controller that compares the set-point temperature and the return-air (indoor) temperature with a dead-band of $1°C$. For example, in the heating mode, if the return-air temperature is $1°C$ lower than the set-point temperature, the heating will turn on and run at full power of $8.4\,kW$ until the set-point is reached. Vice versa for cooling, except that the electric power is $7\,kW$.

To map this controller to our proposed controller, we applied the following strategies:

- As the cooling and heating modes of the HVAC system show different responses, two different I/O datasets for different modes are maintained/updated independently. The controller monitors the mode of the HVAC system and deploys the corresponding I/O dataset to build the proposed controller.
- Recall that the input used in our proposed scheme is electrical power consumption. To achieve a desired power consumption, we convert this desired consumption to a set-point sequence: For example, if the HVAC is in heating mode, and a non-zero desired power consumption is planned, the controller will turn on the heating by giving a set-point that is $2°C$ above the return-air temperature, until the desired energy ($P_{el} * T_s$) is reached (path (b) in Figure 4). Then, the heating is turned off by setting the set-point to the return-air temperature.

In our bi-level predictive control scheme, the Hankel matrices for both heating and cooling modes are built from 200 data-points, with $t_{init} = 10$ and a prediction horizon $n_h = 10$. The controller minimizes electrical power consumption with the following loss function

$$J(y_{pred}, u_{pred}) = \sum_{i}^{N_{pred}} |u_i|$$

To better distinguish the heating and cooling modes in our plots, we use a positive input value for the heating mode and a negative input for the cooling mode. We further enforce the following input constraint to model the maximal power consumption of the heating/cooling.

$$\begin{cases} 0\,kWh \leq u_i \leq 1.5\,kWh, & \text{heating mode} \\ -1.15\,kWh \leq u_i \leq 0\,kWh, & \text{cooling mode} \end{cases}$$

Note that the HVAC unit consumes a constant $2.4\,kW$ of electricity for ventilation, even without heating or cooling. The aforementioned input constraint excludes this basic ventilation power. The parameter $\mathcal{E}_g$ in (13) is set by MATLAB command DIAG(LINSPACE(0.2,0.02,n_c)). The uncertainty set of the weather forecasts is estimated from an analysis of historical data as

$$\mathcal{W} := \left\{ w_i \middle| \begin{bmatrix} -1°C \\ -50W/m^2 \end{bmatrix} \leq w_i \leq \begin{bmatrix} 1°C \\ 50W/m^2 \end{bmatrix} \right\} \qquad (20)$$

B. Experimental Results

In this section, we describe three experiments that were conducted from May 2021 to June 2021. In particular, the first experiment shows the necessity of robust control and the second experiment shows the adaptivity to mode switching. The second one runs a 20-day experiment to show the adaptivity and reliability of the proposed scheme and the final one runs a 4-day experiment to compare the proposed scheme with the default controller. Meanwhile, recall that we use a negative control input to represent cooling and a positive control input for heating, accordingly, and show the control input and system output (indoor temperature) within the same plot to better show the response from input to output.

1) Experiment 1: The first experiment includes two parts: a non-robust version of the proposed scheme (*i.e.* $\mathcal{W} = \{\mathbf{0}\},\ K = \mathbf{O}$) and a robust version with the uncertainty tube given in (20). In this test, we consider a time-varying indoor temperature constraint with respect to office hours, which is relaxed during the night and is tightened to ensure occupant comfort during office hours.

$$\begin{cases} 21°C \leq y_i \leq 26°C, & \text{from 8 a.m. to 6 p.m.} \\ 19°C \leq y_i \leq 30°C, & \text{otherwise} \end{cases}$$

The non-robust experiment was conducted on 14^{th} May 2021 and the result is plotted in Figure 5. The HVAC system was in heating mode throughout this experiment, and we can observe that the heat pump is "off" until it hits the lower bound at around 4 A.M.. Later, it started pre-heating the room to satisfy the office hours temperature constraint at around 6 A.M. However, we can still observe frequent but small constraint violations from 8 A.M. to 10 A.M., which then lead to overheating after 10 A.M.

In comparison, the robust controller effectively handled these issues in an experiment conducted on 25^{th} May 2021. The result is shown in Figure 6, where we used the same time varying indoor temperature constraint. We can observe that the robust controller safely protects the system from violating the lower bound through the whole test, and it also successfully pre-heated the building to fit the time-varying indoor temperature constraint. The performance deterioration that occurred to the non-robust controller after 10 A.M. was avoided as well, where the controller smoothly turned off the heating without unnecessary overheating.

2) Experiment 2: The second experiment is a pilot test to validate the adaptivity to the mode switching and the necessity of active excitation (Algorithm 1). The experiment was conducted from 28^{th} to 29^{th} May 2021, with the result shown in Figure 7, where the indoor temperature of this experiment is bounded within

$$21°C \leq y_i \leq 25°C,$$

This change of heating/cooling mode is depicted as a positive/negative control input and a red/blue shaded region in Figure 7. However, it is noteworthy that the system was in cooling mode on the second evening. If there was no active excitation, the cooling should be off through the night to minimize energy consumption, and the Hankel matrices

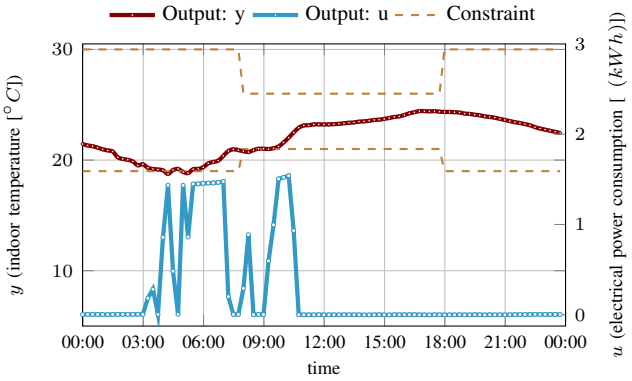

Fig. 5. First experiment in *Polydome*: one-day heating-mode running by the bi-level data-driven control without robust optimization

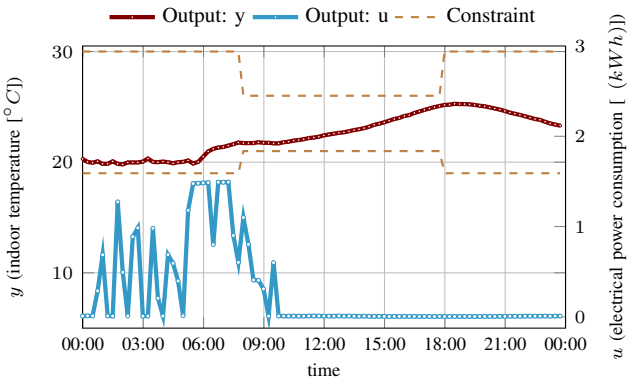

Fig. 6. First experiment in *Polydome*: one-day heating-mode running by the proposed robust data-driven control

used for the controller would have lost persistent excitation. Instead, the active excitation, which is depicted as small fluctuations from 0:00 to 8:00 on the second day, maintained the persistency of excitation. The excitation signal is randomly selected as follows:

$$\begin{cases} 0\,kWh \leq u_{e,i} \leq 0.1\,kWh, & \text{heating mode} \\ -0.075\,kWh \leq u_{e,i} \leq 0\,kWh, & \text{cooling mode} \end{cases}$$

In conclusion, the controller successfully carried out the task of energy minimization in this experiment. In particular, when there is no need for heating/cooling, such as during the second evening, only active excitation took effect to maintain persistency of excitation. The heating/cooling also takes effect to robustly maintain the indoor temperature within the constraints.

3) Experiment 3: This experiment was planned to validate the long-term reliability and adaptivity of the proposed controller. The experiment ran continuously for 20 days from 10^{th} June 2021 to 30^{th} June 2021. The statistics of this experiment is summarized in Table III, and we only plot results from the 20^{th} 12:00 to the 30^{th} 12:00 in Figure 8 to Figure 9 due to the space limit [7].

Note that the weather varies a lot throughout this experiment, with the outdoor temperature even once surpassing $29°C$ on the 20^{th} and also once dropping below $15°C$ on the 26^{th}. Therefore, the experiment shows the adaptivity of the proposed controller to weather variation. Moreover, the cooling mode dominated the whole experiment, with only a few days of heating at night. The proposed controller gives a long-term guarantee of temperature constraint satisfaction (see Table III), while updating the Hankel matrices constantly. Regarding the data update, the active excitation scheme (Algorithm 1) also occasionally took effect to ensure persistency of excitation, such as 00:00 - 6:00 A.M. on 17^{th} June.

[7]Full plots of 20-day experiment are available on Github:https://github.com/YingZhaoleo/Building_results

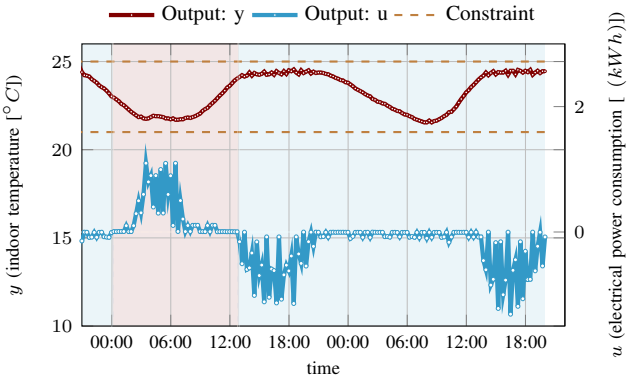

Fig. 7. Second experiment in *Polydome*: two-day running by the proposed robust data-driven control

average indoor temperature	average outdoor temperature	average solar radiation	duration of constraint violation	average hourly power comsumption
$23.7°C$	$20.8°C$	$0.21W/m^2$	$0h$	$1.6kWh$
min/max indoor temperature	min/max outdoor temperature	min/max solar radiation	hours of heating	hours of cooling
$21.5°C$ $24.88°C$	$14.6°C$ $29.5°C$	$0W/m^2$ $0.89W/m^2$	$48h$	$432h$

TABLE III
STATISTICS OF THE 20-DAY EXPERIMENT

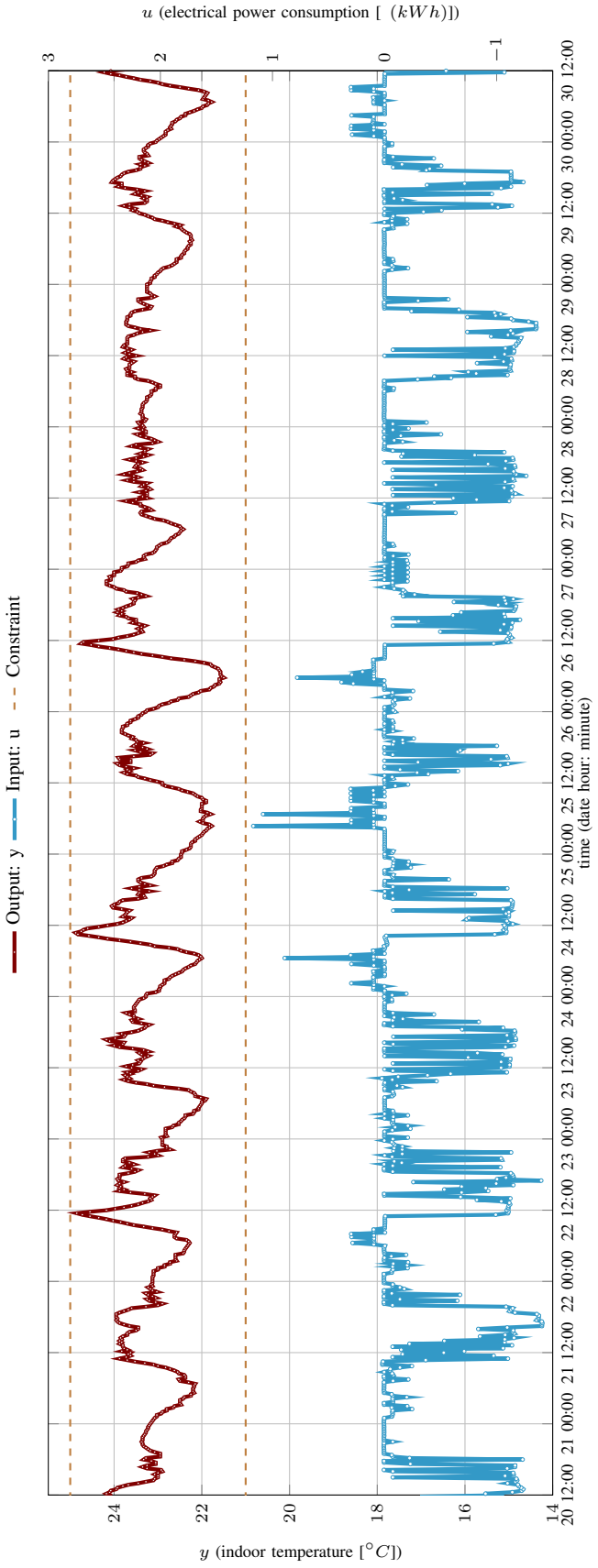

Fig. 8. Experimental results from noon $\mathbf{20}^{th}$ June 2021 to noon $\mathbf{30}^{th}$ June 2021: indoor temperature and electrical power consumption

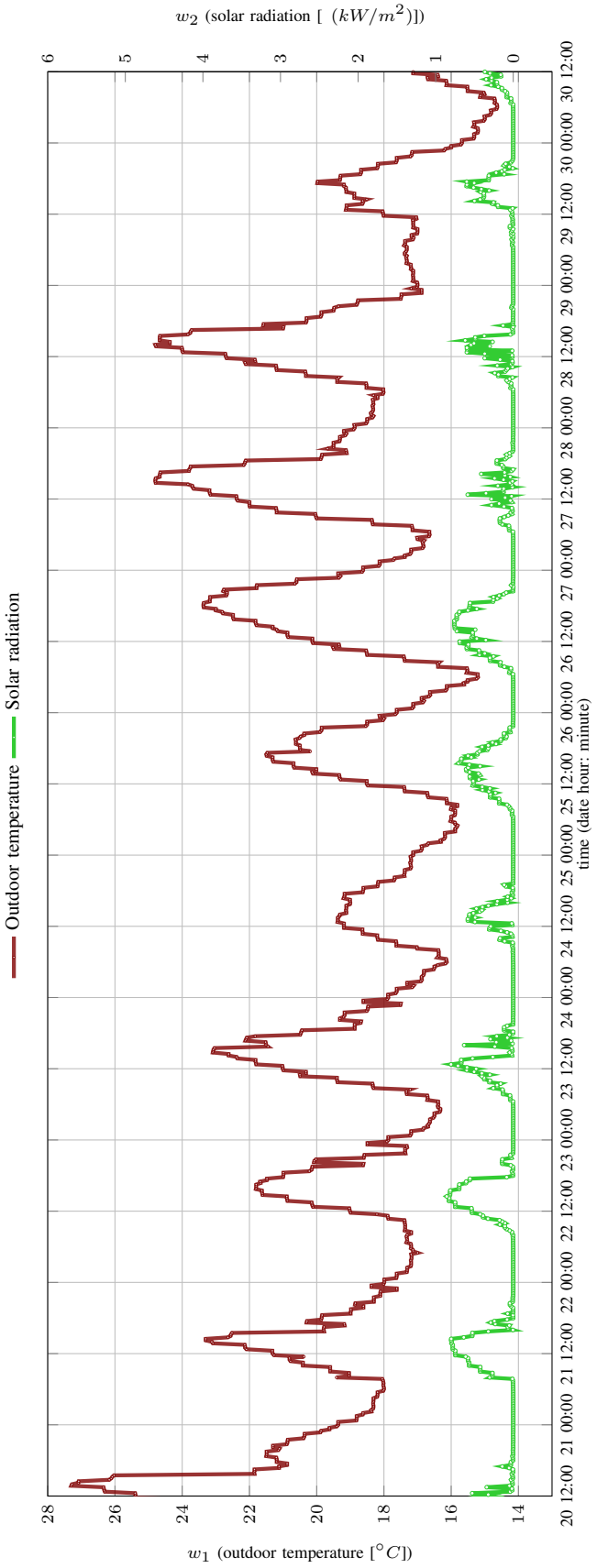

Fig. 9. Experimental results from noon $\mathbf{20}^{th}$ June 2021 to noon $\mathbf{30}^{th}$ June 2021: outdoor temperature and solar radiation

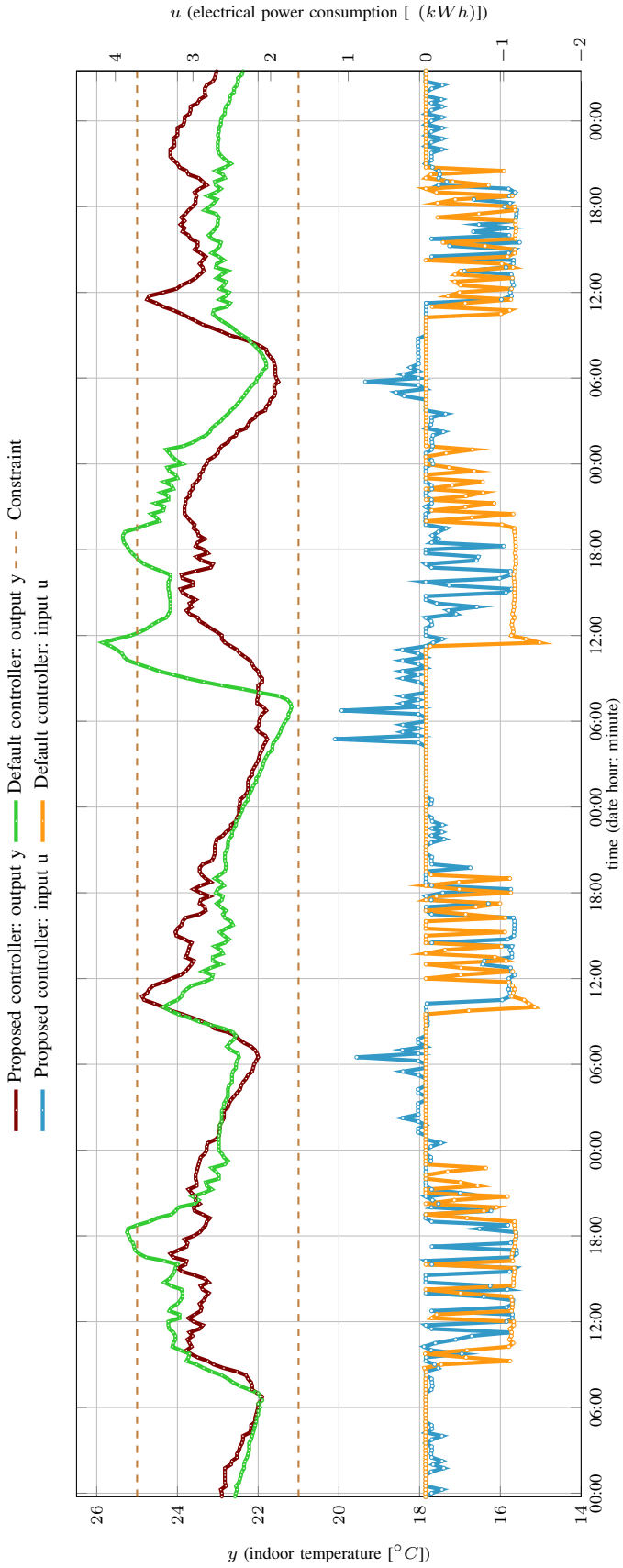

Fig. 10. Comparison of the proposed robust controller and default controller: indoor temperature and electrical power consumption

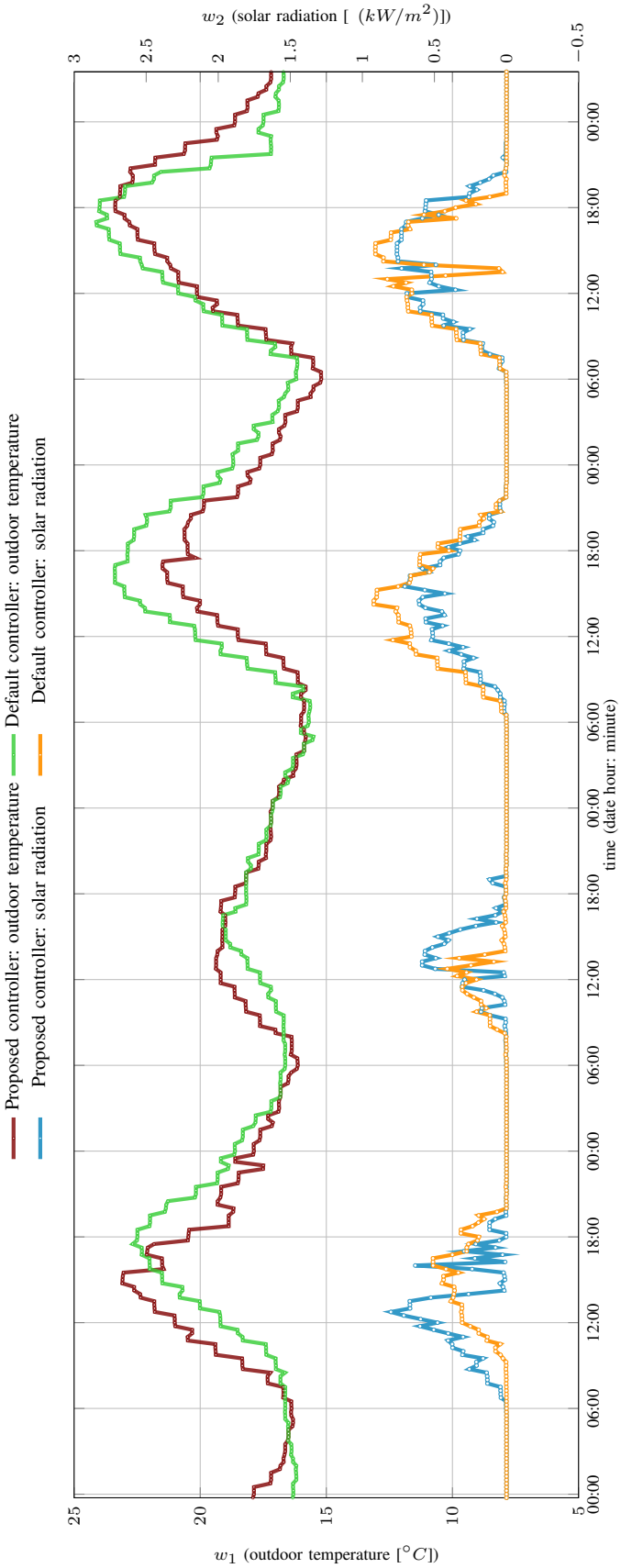

Fig. 11. Comparison of the proposed robust controller and default controller: outdoor temperature and solar radiation

4) Experiment 4: Finally, we compare the proposed robust DeePC scheme with the default controller (Section. VI-A), which regulates the supply air temperature based on the return air temperature. A fixed setpoint at $22°C$ is given to the default controller in order to ensure the occupants' comfort throughout the day. It is worth noting that the default controller is a benchmark controller widely used in the building control community [5], [27], [53].

The experiment with the proposed controller was conducted from 23^{rd} July 2021 to 26^{th} July 2021, and the one with the default controller ran from 7^{th} July 2021 to 10^{th} July 2021. To ensure a fair comparison, the weather conditions for these two experiments were similar, as shown in Figure 11. The indoor temperature and electrical power consumption are plotted in Figure 10, alongside the statistics of these two experiments summarized in Table IV.

From Table IV and Figure 10, more constraint violation is observed from the default controller than the proposed controller. One major underlying reason is that the default controller runs without the knowledge of a weather forecast and only cooled down the building when the return air temperature reached $23°C$. We believe that is the reason accounting for the constraint violation in the day-1 experiment of the default controller. If the default controller could have predicted a high solar radiation and turned the cooling on constantly, the temperature constraint violation should have been avoided.

Besides the benefit of robust constraint satisfaction, the proposed controller is also more power efficient than the default controller under similar weather conditions, which in particular consumed 18.4% less electricity than the default controller (Table IV). Note that, to maintain the data quality, the proposed controller ran the active excitation scheme (Algorithm 1) regularly from 00:00 to 9:00. Thus, there is still the possibility to further improve the energy efficiency of the proposed controller.

	average indoor temperature	average outdoor temperature	average solar radiation	duration of constraint violation
Proposed controller	$23.1°C$	$18.5°C$	$0.17W/m^2$	$0h$
Default controller	$23.2°C$	$18.8°C$	$0.17W/m^2$	$5.75h$
	min/max indoor temperature	min/max outdoor temperature	min/max solar radiation	averaged hourly power comsumption
Proposed controller	$21.5°C$ $24.9°C$	$15.2°C$ $23.4°C$	$0W/m^2$ $0.80W/m^2$	$1.15kWh$
Default controller	$21.2°C$ $25.9°C$	$15.5°C$ $24.1°C$	$0W/m^2$ $0.92W/m^2$	$1.41kWh$

TABLE IV
STATISTICS OF THE FOUR-DAY COMPARISON

VII. CONCLUSION

In this work, we propose a robust bi-level data-driven adaptive-predictive building controller based on the Willems' fundamental lemma. The proposed scheme performs comparably to a classical model-based approach in a numerical simulation. The practical viability is shown by deploying the proposed scheme to a conference building on the EPFL campus, where, without extra modeling effort, our proposed scheme improve 18% energy efficiency and robustly ensures occupant comfort.

REFERENCES

[1] Emu electronics ag. `https://www.emuag.ch/`. Accessed: 2021-06-01.

[2] Influxdb. `https://www.influxdata.com`. Accessed: 2021-06-01.

[3] Tomorrow.io. `https://www.tomorrow.io`. Accessed: 2021-06-01.

[4] Z. Afroz, G. Shafiullah, T. Urmee, and G. Higgins. Modeling techniques used in building hvac control systems: A review. *Renewable and sustainable energy reviews*, 83:64–84, 2018.

[5] A. Aswani, N. Master, J. Taneja, D. Culler, and C. Tomlin. Reducing transient and steady state electricity consumption in hvac using learning-based model-predictive control. *Proceedings of the IEEE*, 100(1):240–253, 2011.

[6] A. Ben-Tal, L. El Ghaoui, and A. Nemirovski. *Robust optimization*. Princeton university press, 2009.

[7] J. Berberich and F. Allgöwer. A trajectory-based framework for data-driven system analysis and control. In *2020 European Control Conference (ECC)*, pages 1365–1370. IEEE, 2020.

[8] J. Berberich, A. Koch, C. W. Scherer, and F. Allgöwer. Robust data-driven state-feedback design. In *2020 American Control Conference (ACC)*, pages 1532–1538. IEEE, 2020.

[9] J. Berberich, J. Köhler, M. A. Müller, and F. Allgöwer. Robust constraint satisfaction in data-driven mpc. In *2020 59th IEEE Conference on Decision and Control (CDC)*, pages 1260–1267. IEEE, 2020.

[10] J. Berberich, J. Köhler, M. A. Müller, and F. Allgöwer. Data-driven model predictive control: closed-loop guarantees and experimental results. *at-Automatisierungstechnik*, 69(7):608–618, 2021.

[11] A. Bisoffi, C. De Persis, and P. Tesi. Data-based stabilization of unknown bilinear systems with guaranteed basin of attraction. *Systems & Control Letters*, 145:104788, 2020.

[12] A. Boodi, K. Beddiar, M. Benamour, Y. Amirat, and M. Benbouzid. Intelligent systems for building energy and occupant comfort optimization: A state of the art review and recommendations. *Energies*, 11(10):2604, 2018.

[13] S. Boyd, S. P. Boyd, and L. Vandenberghe. *Convex optimization*. Cambridge university press, 2004.

[14] D. A. Bristow, M. Tharayil, and A. G. Alleyne. A survey of iterative learning control. *IEEE control systems magazine*, 26(3):96–114, 2006.

[15] G. T. Costanzo, S. Iacovella, F. Ruelens, T. Leurs, and B. J. Claessens. Experimental analysis of data-driven control for a building heating system. *Sustainable Energy, Grids and Networks*, 6:81–90, 2016.

[16] J. Coulson, J. Lygeros, and F. Dörfler. Data-enabled predictive control: In the shallows of the deepc. In *2019 18th European Control Conference (ECC)*, pages 307–312. IEEE, 2019.

[17] J. Coulson, J. Lygeros, and F. Dörfler. Regularized and distributionally robust data-enabled predictive control. In *2019 IEEE 58th Conference on Decision and Control (CDC)*, pages 2696–2701. IEEE, 2019.

[18] C. De Persis and P. Tesi. Formulas for data-driven control: Stabilization, optimality, and robustness. *IEEE Transactions on Automatic Control*, 65(3):909–924, 2019.

[19] S. Dempe. *Foundations of bilevel programming*. Springer Science & Business Media, 2002.

[20] F. Dörfler. Data-enabled predictive control of autonomous energy systems, 2019.

[21] D. Dowson and B. Landau. The fréchet distance between multivariate normal distributions. *Journal of multivariate analysis*, 12(3):450–455, 1982.

[22] J. Drgoňa, J. Arroyo, I. C. Figueroa, D. Blum, K. Arendt, D. Kim, E. P. Ollé, J. Oravec, M. Wetter, D. L. Vrabie, et al. All you need to know about model predictive control for buildings. *Annual Reviews in Control*, 2020.

[23] E. Elokda, J. Coulson, P. Beuchat, J. Lygeros, and F. Dörfler. Data-enabled predictive control for quadcopters. 2019.

[24] P. M. Esfahani and D. Kuhn. Data-driven distributionally robust optimization using the wasserstein metric: Performance guarantees and tractable reformulations. *Mathematical Programming*, 171(1):115–166, 2018.

[25] M. K. S. Faradonbeh, A. Tewari, and G. Michailidis. Input perturbations for adaptive control and learning. *Automatica*, 117:108950, 2020.

[26] W. Favoreel, B. De Moor, and M. Gevers. Spc: Subspace predictive control. *IFAC Proceedings Volumes*, 32(2):4004–4009, 1999.

[27] R. Godina, E. M. Rodrigues, E. Pouresmaeil, and J. P. Catalão. Optimal residential model predictive control energy management performance with pv microgeneration. *Computers & Operations Research*, 96:143–156, 2018.

[28] G. H. Golub and C. Van Loan. Total least squares. In *Smoothing Techniques for Curve Estimation*, pages 69–76. Springer, 1979.

[29] G. H. Golub and C. F. Van Loan. Matrix computations. edition, 1996.

[30] L. Huang, J. Coulson, J. Lygeros, and F. Dörfler. Decentralized data-enabled predictive control for power system oscillation damping. *arXiv preprint arXiv:1911.12151*, 2019.

[31] Y. Lian and C. N. Jones. From system level synthesis to robust closed-loop data-enabled predictive control. *arXiv preprint arXiv:2102.06553*, 2021.

[32] Y. Lian and C. N. Jones. Nonlinear data-enabled prediction and control. *arXiv preprint arXiv:2101.03187*, 2021.

[33] J. Löfberg. *Minimax approaches to robust model predictive control*, volume 812. Linköping University Electronic Press, 2003.

[34] M. Maasoumy, B. Moridian, M. Razmara, M. Shahbakhti, and A. Sangiovanni-Vincentelli. Online simultaneous state estimation and parameter adaptation for building predictive control. In *Dynamic Systems and Control Conference*, volume 56130, page V002T23A006. American Society of Mechanical Engineers, 2013.

[35] G. Marafioti, R. R. Bitmead, and M. Hovd. Persistently exciting model predictive control. *International Journal of Adaptive Control and Signal Processing*, 28(6):536–552, 2014.

[36] I. Markovsky and P. Rapisarda. On the linear quadratic data-driven control. In *2007 European Control Conference (ECC)*, pages 5313–5318. IEEE, 2007.

[37] I. Markovsky and P. Rapisarda. Data-driven simulation and control. *International Journal of Control*, 81(12):1946–1959, 2008.

[38] M. Minakais, S. Mishra, and J. T. Wen. Groundhog day: Iterative learning for building temperature control. In *2014 IEEE International Conference on Automation Science and Engineering (CASE)*, pages 948–953. IEEE, 2014.

[39] E. Mocanu, D. C. Mocanu, P. H. Nguyen, A. Liotta, M. E. Webber, M. Gibescu, and J. G. Slootweg. On-line building energy optimization using deep reinforcement learning. *IEEE transactions on smart grid*, 10(4):3698–3708, 2018.

[40] H. Neudecker. A matrix trace inequality. *Journal of mathematical analysis and applications*, 166(1):302–303, 1992.

[41] J. Nocedal and S. Wright. *Numerical optimization*. Springer Science & Business Media, 2006.

[42] J. G. Rueda-Escobedo and J. Schiffer. Data-driven internal model control of second-order discrete volterra systems. In *2020 59th IEEE Conference on Decision and Control (CDC)*, pages 4572–4579. IEEE, 2020.

[43] G. W. Stewart. *Matrix Algorithms: Volume 1: Basic Decompositions*. SIAM, 1998.

[44] R. S. Sutton and A. G. Barto. *Reinforcement learning: An introduction*. MIT press, 2018.

[45] A. Swales et al. Open modbus/tcp specification. *Schneider Electric*, 29:3–19, 1999.

[46] M. Tesfay, F. Alsaleem, P. Arunasalam, and A. Rao. Adaptive-model predictive control of electronic expansion valves with adjustable setpoint for evaporator superheat minimization. *Building and Environment*, 133:151–160, 2018.

[47] H. J. van Waarde and M. K. Camlibel. A matrix finsler's lemma with applications to data-driven control. *arXiv preprint arXiv:2103.13461*, 2021.

[48] H. J. Vanwaarde, M. K. Camlibel, and M. Mesbahi. From noisy data to feedback controllers: non-conservative design via a matrix s-lemma. *IEEE Transactions on Automatic Control*, 2020.

[49] J. C. Willems and J. W. Polderman. *Introduction to mathematical systems theory: a behavioral approach*, volume 26. Springer Science & Business Media, 1997.

[50] J. C. Willems, P. Rapisarda, I. Markovsky, and B. L. De Moor. A note on persistency of excitation. *Systems & Control Letters*, 54(4):325–329, 2005.

[51] L. Xu, M. S. Turan, B. Guo, and G. Ferrari-Trecate. A data-driven convex programming approach to worst-case robust tracking controller design. *arXiv preprint arXiv:2102.11918*, 2021.

[52] X. Yan, Q. Ren, and Q. Meng. Iterative learning control in large scale hvac system. In *2010 8th World Congress on Intelligent Control and Automation*, pages 5063–5066. IEEE, 2010.

[53] S. Yang, M. P. Wan, W. Chen, B. F. Ng, and S. Dubey. Model predictive control with adaptive machine-learning-based model for building energy efficiency and comfort optimization. *Applied Energy*, 271:115147, 2020.

[54] M. Yin, A. Iannelli, and R. S. Smith. Maximum likelihood estimation in data-driven modeling and control. *arXiv preprint arXiv:2011.00925*, 2020.

[55] Y. Yu, S. Talebi, H. J. van Waarde, U. Topcu, M. Mesbahi, and B. Açıkmeşe. On controllability and persistency of excitation in data-driven control: Extensions of willems' fundamental lemma. *arXiv preprint arXiv:2102.02953*, 2021.